

# Light-Control of Localised Photo-Bio-Convection

Jorge Arrieta,<sup>1</sup> Marco Polin,<sup>2</sup> Ramón Saleta-Piersanti,<sup>1</sup> and Idan Tuval<sup>1</sup>

<sup>1</sup>*Instituto Mediterráneo de Estudios Avanzados, IMEDEA, UIB-CSIC, Esporles, 07190, Spain*

<sup>2</sup>*Physics Department and Centre for Mechanochemical Cell Biology,  
University of Warwick, Gibbet Hill Road, Coventry, CV4 7AL, United Kingdom*

(Dated: May 17, 2022)

Microorganismal motility is often characterised by complex responses to environmental physico-chemical stimuli. Although the biological basis of these responses is often not well understood, their exploitation already promises novel avenues to directly control the motion of living active matter at both the individual and collective level. Here we leverage the phototactic ability of the model microalga *Chlamydomonas reinhardtii* to precisely control the timing and position of localised cell photo-accumulation, leading to the controlled development of isolated bioconvective plumes. This novel form of photo-bio-convection allows a precise, fast and reconfigurable control of the spatio-temporal dynamics of the instability and the ensuing global recirculation, which can be activated and stopped in real time. A simple continuum model accounts for the phototactic response of the suspension and demonstrates how the spatio-temporal dynamics of the illumination field can be used as a simple external switch to produce efficient bio-mixing.

The autonomous movement of microorganisms has fascinated scientists since the discovery of the microbial world. Particularly striking is the variety of coordinated collective dynamics that emerges with startling reliability in groups of motile microorganisms, from traffic lanes and oscillations in bacterial swarms [1, 2], to wolf-pack hunting [3] and microbial morphogenesis [4, 5]. Nowadays, microbial motility is an important part of a growing interdisciplinary field aiming to uncover the fundamental laws governing the dynamics of so-called active matter [6], eventually allowing us to harness micron-scale motility for applications ranging from targeted payload delivery [7] to direct assembly of materials [8, 9], with either living organisms or synthetic microswimmers [10–12]. Realising this potential will hinge on our ability to alter and ultimately control the motion of both individual cells and microbial collectives.

Microbial motility can be controlled through clever engineering of boundaries [13–15] or topology [16, 17] of the vessels holding the microbial suspension, leading for example to predictable accumulation [18–20] or circulation of cells [14, 21–23]. However, together with strategies squarely rooted in physics, control of living microswimmers can rely also on approaches bridging between physics and biology, by taking advantage of pathways linking motility with the perception of physico-chemical stimuli by cells. Light is particularly well suited to this end: its manipulation is readily achievable at both the macroscopic and microscopic [24, 25] scales; and it is an important stimulus for a wide variety of microorganisms, providing both energy [26] and information often used to prevent potentially lethal light-induced stress [27]. Most microorganisms respond to light by linking swimming speed to light intensity (photokinesis, [28]) and/or re-directing their motion towards or away from the light source (phototaxis, [29–31]). Although the physiological details underpinning these active re-

sponses are often not completely understood [30–33], techniques employing light to precisely control the dynamics of swimming microorganisms are already emerging. Biological responses to light led to the development of genetically-engineered light-sensitive bacteria [34–36] used, for example, to power micron-size motors [23], and have even inspired the fabrication of light-reactive artificial swimmers [11, 37–39].

Within eukaryotes together with recent studies on *Euglena gracilis* (Protozoa) [40–43], current applications focus in particular on the model unicellular green alga *Chlamydomonas reinhardtii* (CR), and range from micro-cargo delivery by individual cells [44] to trapping of passive colloids by light-induced hydrodynamic tweezers [45], and photofocussing of algal suspensions through an interplay of photo- and gyro-taxis [46]. Unlocking the full potential of light-based control, however, will require the development of techniques based on a collective response that is both quick and localised. Despite considerable progress, this is not currently available.

Here we exploit the phototactic response of CR to

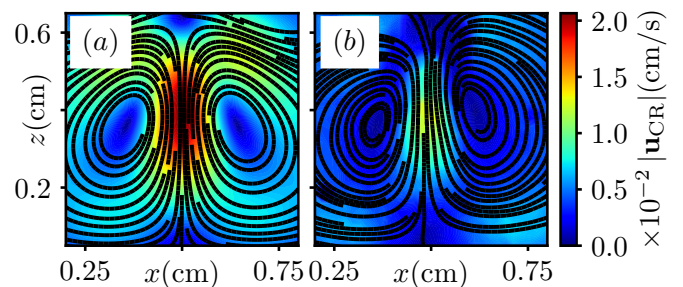


FIG. 1. Contours of the cells averaged velocity field obtained from (a) the numerical integration of (1)–(3) for  $n_0 = 1.5 \times 10^7$  cells/ml and  $\beta = 0.14$  and (b) from the PIV analysis of experimental data. Solid black lines represent in both panels the corresponding streamlines.

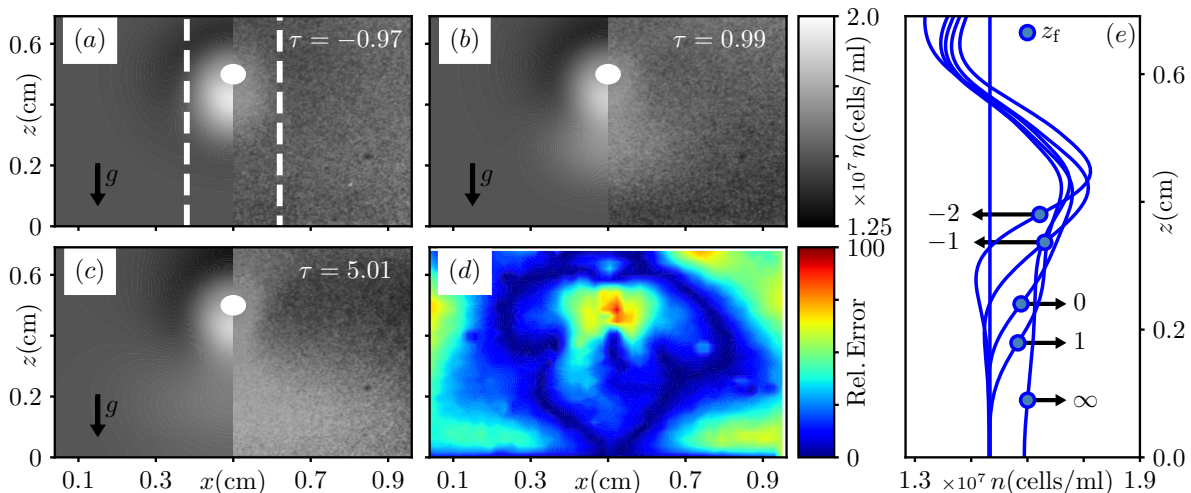


FIG. 2. Dynamics of plume formation. (a-c) Evolution of photo-accumulation and plume formation at different values of the normalized time  $\tau$ . Panels show the cell density from the continuum model,  $n$  (left-side), and the dark-field image from the corresponding experiment at the same value of  $\tau$ . White dots in (a-c) correspond with the position of the light fibre. (d) Relative error between experimental and numerical flows of cells (each flow field has been first rescaled by its maximum value). (e) Average vertical cell concentration profiles for the specified values of  $\tau$ , together with the positions of  $z_f$  (circles).

demonstrate a novel form of dynamic control of a cell suspension, based on a fast ( $\sim 10$  s) accumulation that can be localised anywhere within the suspension. Cells photo-accumulate around the light from a horizontal optical fibre (Fig. 1b) and act as a miniaturised pump driving a global recirculation of the suspension with a fast response time, quantitatively captured by a simple model (Fig. 1a). The fast response of the suspension can be exploited for efficient bio-mixing, an attractive solution to improve current photo-bio-reactor technology for biofuel production where mixing is essential to distribute nutrients, metabolites and heat and to transfer gases across gas-liquid interfaces [47–49]. Our results serve as a proof-of-principle for more complex instances of light-controlled fluid flows in biological suspensions.

Unicellular biflagellate green algae *Chlamydomonas reinhardtii* wild type strain CC125 were grown axenically at  $20^\circ\text{C}$  in Tris-Acetate-Phosphate medium (TAP) [50] under fluorescent light illumination (OSRAM Fluora,  $100\ \mu\text{mol}/\text{m}^2\text{s}$  PAR) following a 14 h/10 h light/dark diurnal cycle. Exponentially growing cells were harvested, photo-accumulated, diluted to the target concentration with fresh TAP, and loaded in a vertical observation chamber formed by a square shaped Agar-TAP gasket of  $L = 1\ \text{cm}$  side and  $h = 1\ \text{mm}$  thickness, sandwiched between two coverslips. The main experiments were performed at two average concentrations:  $n_0^h = 1.5 \times 10^7\ \text{cells}/\text{ml}$  (8 repeats); and  $n_0^l = 7 \times 10^6\ \text{cells}/\text{ml}$  (6 repeats). Tests for plume formation were also conducted at  $n_0 = 6.1, 9.0 \times 10^6; 1.24, 1.40 \times 10^7\ \text{cells}/\text{ml}$ . The dynamics of the suspension was visualised through darkfield illumination at 635 nm (FLDR-i70A-R24, Falcon Light-

ing Germany) and recorded by a CCD camera (Pike, AVT USA) hosted on a continuously focusable objective (InfiniVar CFM-2S, Infinity USA). Localised actinic illumination was provided by a  $200\ \mu\text{m}$ -diameter horizontal multimode optical fibre (FT200EMT, Thorlabs USA) coupled to a 470 nm high-power LED (M470L2, Thorlabs USA). The fibre’s output intensity  $I(\mathbf{x})$ , centred at  $\mathbf{x}_{\text{fb}} = (x_{\text{fb}}, z_{\text{fb}})$  (see Fig. 2a), is well approximated by a Gaussian (width  $\sigma_I = 667\ \mu\text{m}$ ; peak intensity  $I_0 = 260\ \mu\text{mol}/\text{m}^2\text{s}$ ), which will be used in numerical simulations throughout the manuscript.

Figure 2 shows the evolution of the photo-accumulation dynamics for  $n_0^h$ . In the absence of light stimuli, individual cells swim in a characteristic run-and-tumble-like behaviour [51] leading to a uniform spatial distribution at the population level (Fig. 2a). As the actinic light is switched on, phototactic cells start accumulating around the fibre, through a characteristic phototactic steering mechanism [33] based on an interplay between time-dependent stimulation of a light-sensitive organelle [52, 53] and the ensuing flagellar response [54]. Phototaxis leads, within  $\sim 10$  s, to a  $\sim 2\ \text{mm}$ -wide region of high cell concentration [31]. This is gravitationally unstable, and eventually falls forming a single, localised sinking plume of effectively denser fluid (Fig. 2b-d and Supplementary Movie S1). The system converges to its steady state as the plume reaches the bottom of the container ( $\sim 30$  s), two orders of magnitude faster than reported for alternative configurations [45] with the cells advected along the strong global recirculation seen in Fig. 1a (experimental flow of cells obtained with Open-PIV using cells as tracers [55]). This buoyancy-driven

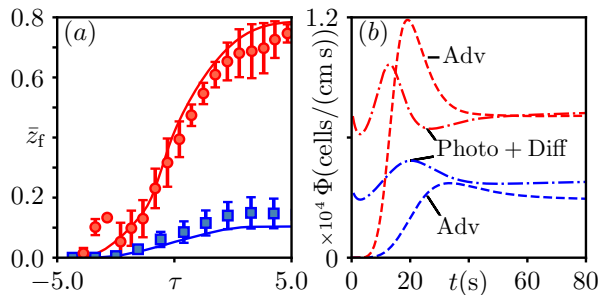


FIG. 3. Plume falling and flux balance. (a) Time evolution of the experimental (circles/squares) and numerical (solid lines) fronts as a function of  $\tau$ , for  $z_{fb} \sim 0.5$  cm. Simulations were run with  $n_0 = 1.5 \times 10^7$  cells/ml (red line) and  $n_0 = 7.0 \times 10^6$  cells/ml (blue line) with all other parameters as described in the text. (b) Evolution of the advective (dashed lines) and phototactic plus diffusive (dot-dashed lines) fluxes across a circular control surface of radius 0.18 cm for the two cases described in panel (a). Same colour code.

instability is reminiscent of bioconvection, one of the best known examples of collective behaviour in suspensions of microswimmers [56–58]. As discussed below, it can be understood as a light-induced instance of a single bioconvective plume, which can be actively modulated by light and localised anywhere within the sample. Cell accumulation, however, does not always lead to a plume. In samples with average concentration  $n_0^h$ , the photo-accumulated high-concentration region does not sink to the bottom but reaches instead a stable height just below the fibre’s centre. Despite the absence of a proper plume, however, the background fluid is still globally stirred (see Supplementary Movie S2).

The sinking dynamics of the initial region of photo-accumulated cells, can be quantified from the average vertical profile of the recorded images within a 2 mm-wide strip around  $x_{fb}$  (Fig. 2a). The position of the profile’s maximal vertical derivative,  $z_f$ , provides a faithful measure of the height of the photo-accumulated front, which is easy to follow in time (Fig. 2e). A heuristic description of its dynamics through the sigmoid function  $z_f(t) - z_f(0) = z_f^\infty \exp[(t - t_0)/\delta] / (\exp[(t - t_0)/\delta] + 1)$  can be used for both temporal registration, through a parameter to set a common origin of time  $t_0$ ; and rescaling, by the characteristic falling time  $\delta$ . Typically,  $\delta = 15.5 \pm 6.6$  s for  $n_0^h$ , and  $2.4 \pm 1.1$  s for  $n_0^l$ . Figure 3a shows the average rescaled front dynamics  $\bar{z}_f(\tau) = (z_f(\tau) - z_f(0)) / z_f(0)$  in terms of the intrinsic time  $\tau = (t - t_0) / \delta$ . We see that the front falls almost to the bottom of the sample ( $\bar{z}_f = 1$ ) in the high concentration case ( $n_0^h$  blue circles) while in the low concentration case ( $n_0^l$  red circles) the steady-state position is just  $\sim 1$  mm below the fibre ( $\bar{z}_f \simeq 0.1$ ). This hints at the existence of a bifurcation as the average concentration is increased from  $n_0^l$  to  $n_0^h$ .

The behaviour of the system, and the presence of a

bifurcation, can be rationalised through a simple continuum model of 2D photo-bioconvection. The model describes the coupling between the local cell density,  $n(\mathbf{x}, t)$ , and the fluid flow,  $\mathbf{u}(\mathbf{x}, t)$  ( $\mathbf{x} = (x, z)$ ). The former obeys a continuity equation which includes contributions from the cells’ active diffusion, phototaxis, and advection by the local background flow. The latter follows the Navier-Stokes equations, which couple to  $n(\mathbf{x}, t)$  through the cells’ excess density ( $\Delta\rho$ ) over the surrounding fluid of density  $\rho_F$ . Following previous work [56, 57] this is captured here in the Boussinesq approximation. We will exclude gravitaxis [56], gyrotaxis [59], and the effect of cells’ activity in both the bulk stress and the cell diffusivity tensors [57, 59]: although essential for several phenomena, ranging from spontaneous bioconvection [57–59] to cells’ focussing [46], they do not appear to play a significant role here in determining either the emergence and falling dynamics of a plume or the geometric structure of the ensuing recirculation, and in the spirit of a minimal-model approach will not be considered. We note, however, that they could still contribute to a global rescaling of the dynamics. The system, contained within a square cavity of side  $L$ , is then described by the following set of equations:

$$\nabla \cdot \mathbf{u} = 0, \quad (1)$$

$$\frac{\partial \mathbf{u}}{\partial t} + \mathbf{u} \cdot \nabla \mathbf{u} = -\nabla p - n\hat{z} + \sqrt{\frac{Sc}{Ra}} \nabla^2 \mathbf{u}, \quad (2)$$

$$\frac{\partial n}{\partial t} + \nabla \cdot [(\mathbf{u} + \mathbf{u}_{ph})n] = \frac{1}{\sqrt{Ra Sc}} \nabla^2 n, \quad (3)$$

with no-slip at the boundary, and no cell flux through the boundary. Despite using the same symbols for convenience, Eqs. (1-3) have been non-dimensionalised by using  $L$  as the characteristic length, and introducing the characteristic velocity for buoyancy-driven flow,  $v_c = (n_0 g \Delta\rho V_{CR} L / \rho_F)^{1/2}$ , where  $V_{CR} = 4\pi r_{CR}^3 / 3$  is the estimated volume of an individual cell assuming a sphere of radius  $r_{CR}$ . The characteristic time is then  $t_c = L / v_c$ ; the scale for the (2D) pressure  $p$ , is given by  $h\rho_F v_c^2$ ; and  $n_0$  rescales the cell density. The behaviour of the system is dictated by three non-dimensional numbers: a Rayleigh number,  $Ra = (v_c L)^2 / \nu D$ , and a Schmidt number,  $Sc = \nu / D$ , based on the kinematic viscosity of the fluid ( $\nu$ ) and the cells’ effective diffusivity ( $D$ ); and the phototactic sensitivity  $\beta$ , which governs the non-dimensional phototactic term,  $\mathbf{u}_{ph} = \beta(v_s / v_c)(|\mathbf{x} - \mathbf{x}_{fb}| / h^*) \nabla I / |\nabla I|_{max}$ . The phototactic drift, derived and tested in [31], includes the cells’ swimming speed,  $v_s = 7.8 \times 10^{-3}$  cm/s, and the effective thickness of the illuminated chamber,  $h^* = 5.19 \times 10^{-2}$  cm. The experimental system is expected to correspond to  $\beta = 0.14$  [31]. Other parameters are fixed to:  $\Delta\rho = 0.05$  g/cm<sup>3</sup>;  $\rho_F = 1$  g/cm<sup>3</sup>;  $\nu = 10^{-2}$  cm<sup>2</sup>/s;  $r_{CR} = 5 \times 10^{-4}$  cm;  $D = 3.9 \times 10^{-4}$  cm<sup>2</sup>/s [31, 51]. Cells are initially uniformly distributed within the quiescent fluid, and the vorticity-stream function formula-

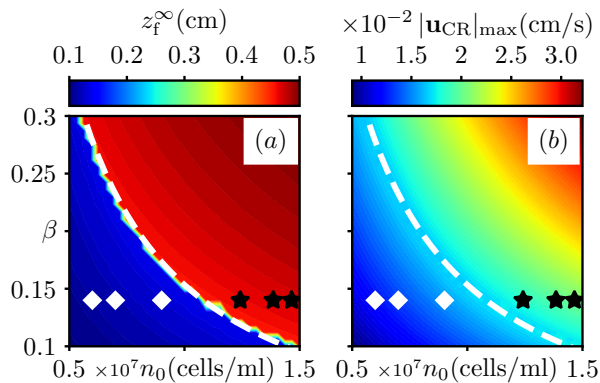


FIG. 4. Photo-bio-convective phase behaviour. (a) Final position of the plume front,  $z_f^\infty$  and, (b) maximum velocity of the cells,  $|\mathbf{u}_{\text{CR}}|_{\text{max}}$ , as function of the initial cell density  $n_0$  and photo-adaptation parameter  $\beta$ . Plume forming/non-forming experiments are indicated by black squares/white diamonds respectively. The isoline  $|\mathbf{u}_{\text{CR}}|_{\text{max}} = 1.66 \times 10^{-2}$  cm/s separates not-falling/falling regimes (white dashed line).

tions of Eqs. (1-3) are integrated with a spatially centred, second-order accurate, finite-difference scheme [60]; at each intermediate stage of the third-order Runge-Kutta method used to advance time, the Laplace equation for the stream function is solved with the conjugate gradient method [61]. The integration scheme was validated by comparison with benchmark solutions [62].

Figure 2 compares the experimental and numerical dynamics of plume formation and sinking, as a function of the reduced time  $\tau$  (here for  $z_{\text{fb}} = 0.5$  cm;  $n_0 = n_0^{\text{h}}$ ). The agreement is excellent with no fitting parameters, and it is maintained also at longer times. Figure 2d shows the relative error between cells' stationary velocity field ( $\mathbf{u}_{\text{CR}} = (\mathbf{u} + \mathbf{u}_{\text{ph}})v_c$ ) from experiments and model, rescaled by their peak velocity. The small discrepancy ( $< 25\%$  on average) shows that the model captured well the structure of the photo-bioconvective flow of cells (see also Fig. 1). A closeup, in Fig. 3, on the experimental (circles) and numerical (solid lines) front dynamics, proves that the model captures both the sinking regime at  $n_0^{\text{h}}$ , and non-sinking one at  $n_0^{\text{l}}$ . We therefore decided to explore systematically the system's behaviour *in silico* by performing a parametric sweep in the range  $n_0 \in [0.5, 1.5] \times 10^7$  cells/ml and  $\beta \in [0.1, 0.3]$ . Figure 4a,b shows that both the characteristic falling time ( $\delta$ ) and the steady-state front position ( $z_f^\infty$ ) indicate the presence of two distinct regimes separated by a sharp transition, in line with experiments (star marks in Fig. 4). There is a low- $n_0$ /low- $\beta$  regime, where the cells accumulate but do not fall; and a high- $n_0$ /high- $\beta$  one, where the light induces a single, isolated bioconvective plume driving a vigorous recirculation across the sample (Fig. 1). The two regimes are separated by a critical curve  $\beta n_0 \approx \text{constant}$ , corresponding to the isoline of maximum cells' velocity,  $|\mathbf{u}_{\text{CR}}|_{\text{max}} \simeq 1.66 \times 10^{-2}$  cm/s.

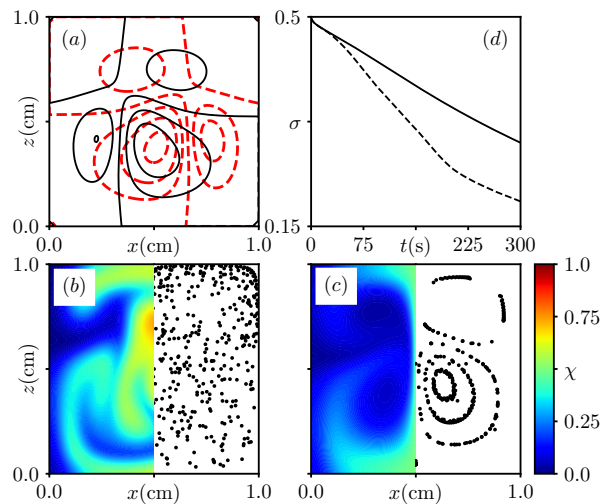


FIG. 5. Mixing by blinking plumes. (a) Streamlines of the induced flow at half a period (black line) and a full period (red line) of the time-dependent light protocol. The spatial distribution of  $\chi$  (left-hand side) at  $t \simeq 200$  s and the Poincaré map (right-hand side) after  $i = 75$  periods for (b) the “blinking plumes” and, (c) the centred stationary case, respectively. (d) Time evolution of the spatial standard deviation of  $\chi$  computed in (b) (dashed line) and (c) (solid line).

This is compatible with the full set of  $n_0$  values explored experimentally (Fig. 4b). The process driving the bifurcation can be understood intuitively by examining the balance between phototactic, diffusive and advective fluxes of cells. Figure 3b shows the evolution of these fluxes across a circle of radius 18 mm centred on the optical fibre. Before the bifurcation (blue) advection (dot-dashed line) is always lower than the net flux due to cell motion (phototaxis and diffusion, dashed line): the front remains close to its initial position. Beyond the bifurcation (red) the downward advective flux becomes dominant shortly after the initial accumulation, and the photo-accumulated cells are transported downwards with a critical velocity arising from flux balance.

The ability to determine location and timing of the plume formation can be harnessed to identify and realise strategies to govern the global transport properties of the suspension. An important example is the possibility to control and accelerate the active biomixing of nutrients. A simple procedure takes advantage of the left-right asymmetric flows generated when the light source is displaced from the mid-point of the chamber, as shown in the streamlines of Fig. 5a for a  $\pm 1.5$  mm shift from the centre (dashed red and solid black lines respectively), and experimentally in Supplementary Movie S3. Alternating evenly between the two plumes in a cycle of period  $T$ , generates flow fields that display the characteristic crossing of streamlines required for efficient mixing in 2D, and realise within a photo-bioconvective context the

blinking vortex, a paradigmatic example of mixing by chaotic advection [63]. Figure 5b,c and Supplementary Movie S4 show how the concentration  $\chi$  of an advected nutrient of diffusivity  $D_\chi = 3 \times 10^{-3} \text{ mm}^2/\text{s}$ , mimicking photosynthetically-important gases like  $\text{CO}_2$  [64], evolves from an initial distribution localised in the right half of the container, for  $t \sim 200 \text{ s}$ . Crossing of streamlines leads to formation, stretching and folding of the thin filaments characteristic of chaotic advection. These in turn cause a significantly faster mixing than for a single steady plume (Fig. 5d), as quantified also through the decay of the standard deviation of the spatial concentration profile,  $\sigma^2 = \langle (\xi - \langle \xi \rangle)^2 \rangle$  (Fig. 5e) [65]. The origin of the enhanced mixing is immediately clear from the Poincaré maps obtained from the trajectories of ten tracer particles initially distributed uniformly along  $z = 5 \text{ mm}$  and followed over  $75 T$  (Fig. 5c,d right panels). Closed quasi-periodic orbits are readily visible for a stationary centred single plume while the “blinking plumes” lead to particles exploring most of the spatial domain. Active light patterning can therefore induce mixing advective maps, leading to strongly enhanced nutrient transport throughout the cell culture.

We have presented a novel mechanism that harnesses phototaxis to actively control a suspensions of swimming microorganisms through their accumulation around a localised light source. The ensuing global instability, characterised by steady vortical flows for all parameter values, can easily lead to the emergence of isolated bioconvective plumes whose spatio-temporal localisation is simply tuned by the external illumination. These properties contrast with the limited control afforded by standard bioconvection [41, 66–69], and enable rapid light-mediated control of the flow which can be used to regulate the transport properties of the suspension. The simple minimal model we use provides a surprisingly accurate quantitative description of the experimental system with no fitting parameters, but only when viewed in terms of the reduced time  $\tau$ . In terms of real time, plumes fall slower in experiments than in simulations:  $\delta = 10.5 \pm 4.7 \text{ s}$  across all experiments beyond the bifurcation, compared to a range  $4.5 \text{ s} - 4.8 \text{ s}$  expected from the model. Interestingly, the quantitative agreement is much improved below the bifurcation (exp:  $\delta = 4.8 \pm 2.5 \text{ s}$ ; num:  $3.1 \text{ s} - 3.7 \text{ s}$ ). The discrepancy beyond the bifurcation is possibly coming from a combination of disregarded swimming features (gravitaxis and gyrotaxis [56, 59]) and confinement [70], to be disentangled in a future, dedicated study. Overall, together with recent work which pioneered the use of emergent radial stress profiles [45], our results set the stage for the future use of light for fast and complex spatio-temporal control of the macroscopic dynamics of phototactic suspensions.

All movies are available on request. We acknowledge the support of the Spanish Ministry of Economy and Competitiveness Grants No. FIS2016-77692-C2-1-P (IT)

and CTM-2017-83774-D (JA), and the subprogram Juan de la Cierva No. IJCI-2015-26955 (JA). JA is extremely grateful to Sara Guerrero for her enormous encouragement and support in the development of this work. MP and IT would like to thank Raymond Goldstein for support in the initial stages of the project.

- 
- [1] C. Chen, S. Liu, X. Q. Shi, H. Chaté, and Y. Wu, *Nature* **542**, 210 (2017).
  - [2] G. Ariel, A. Shklarsh, O. Kalisman, C. Ingham, and E. Ben-Jacob, *New Journal of Physics* **15** (2013), 10.1088/1367-2630/15/12/125019.
  - [3] J. E. Berleman and J. R. Kirby, *FEMS Microbiology Reviews* **33**, 942 (2009).
  - [4] R. L. Chisholm and R. A. Firtel, *Nature Reviews Molecular Cell Biology* **5**, 531 (2004).
  - [5] P. Deng, L. De Vargas Roditi, D. Van Ditmarsch, and J. B. Xavier, *New Journal of Physics* **16**, 1 (2014), NIHMS150003.
  - [6] M. C. Marchetti, J. F. Joanny, S. Ramaswamy, T. B. Liverpool, J. Prost, M. Rao, and R. A. Simha, *Reviews of Modern Physics* **85**, 1143 (2013).
  - [7] N. Koumakis, A. Lepore, C. Maggi, and R. Di Leonardo, *Nature Communications* **4**, 1 (2013).
  - [8] L. Angelani, C. Maggi, M. L. Bernardini, A. Rizzo, and R. Di Leonardo, *Physical Review Letters* **107**, 1 (2011).
  - [9] Z. Ma, Q. L. Lei, and R. Ni, *Soft Matter* **13**, 8940 (2017), 1706.00202.
  - [10] F. Kümmel, P. Shabestari, C. Lozano, G. Volpe, and C. Bechinger, *Soft Matter* **11**, 6187 (2015).
  - [11] C. Bechinger, R. Di Leonardo, H. Löwen, C. Reichhardt, G. Volpe, and G. Volpe, *Reviews of Modern Physics* **88** (2016), 10.1103/RevModPhys.88.045006, 1602.00081.
  - [12] A. Aubret, M. Youssef, S. Sacanna, and J. Palacci, *Nature Physics* (2018), 10.1038/s41567-018-0227-4.
  - [13] P. Denissenko, V. Kantsler, D. J. Smith, and J. Kirkman-Brown, *Proceedings of the National Academy of Sciences* **109**, 8007 (2012).
  - [14] H. Wioland, E. Lushi, and R. E. Goldstein, *New Journal of Physics* **18**, 075002 (2016), 1603.01143.
  - [15] S. Thutupalli, D. Geyer, R. Singh, R. Adhikari, and H. Stone, *Proceedings of the National Academy of Sciences*, 1 (2017), 1710.10300.
  - [16] L. Giomi, *New Journal of Physics* **18** (2016), 10.1088/1367-2630/18/8/081001.
  - [17] A. Morin and D. Bartolo, *Physical Review X* **8**, 21037 (2018), 1803.10782.
  - [18] P. Galajda, J. Keymer, P. M. Chaikin, and R. Austin, *Journal of Bacteriology* **189**, 8704 (2007).
  - [19] V. Kantsler, J. Dunkel, M. Polin, and R. Goldstein, *Proceedings of the National Academy of Sciences of the United States of America* **110** (2013), 10.1073/pnas.1210548110/-/DCSupplemental.
  - [20] T. Ostapenko, F. J. Schwarzendahl, T. J. Bøddeker, C. T. Kreis, J. Cammann, M. G. Mazza, and O. Bäümchen, *Physical Review Letters* **120**, 068002 (2018), 1608.00363.
  - [21] E. Lushi, H. Wioland, and R. E. Goldstein, *Proceedings of the National Academy of Sciences* **111**, 9733 (2014), 1407.3633.
  - [22] A. Bricard, J. B. Caussin, N. Desreumaux, O. Dauchot,

- and D. Bartolo, *Nature* **503**, 95 (2013), 1311.2017.
- [23] G. Vizsnyiczai, G. Frangipane, C. Maggi, F. Saglimbeni, S. Bianchi, and R. Di Leonardo, *Nature Communications* **8**, 15974 (2017).
- [24] S.-H. Lee, Y. Roichman, and D. G. Grier, *Optics Express* **18**, 6988 (2010).
- [25] D. Stellinga, M. E. Pietrzyk, J. M. Glackin, Y. Wang, A. K. Bansal, G. A. Turnbull, K. Dholakia, I. D. Samuel, and T. F. Krauss, *ACS Nano* **12**, 2389 (2018).
- [26] A. N. Dodd, J. Kusakina, A. Hall, P. D. Gould, and M. Hanaoka, *Photosynthesis Research* **119**, 181 (2014).
- [27] Z. Li, S. Wakao, B. B. Fischer, and K. K. Niyogi, *Annual review of plant biology* **60**, 239 (2009).
- [28] D. P. Häder, *Microbiological reviews* **51**, 1 (1987).
- [29] D.-p. Häder and M. Lebert, in *Chemotaxis: methods and protocols*, *Methods in Molecular Biology*, Vol. 571, edited by T. Jin and D. Herold (Humana Press, Totowa, NJ, 2009) Chap. 3, pp. 51–65.
- [30] K. Drescher, R. E. Goldstein, and I. Tuval, *Proceedings of the National Academy of Sciences* **107**, 11171 (2010).
- [31] J. Arrieta, A. Barreira, M. Chioccioli, M. Polin, and I. Tuval, *Scientific Reports* **7**, 3447 (2017), 1611.08224.
- [32] A. Giometto, F. Altermatt, A. Maritan, R. Stocker, and A. Rinaldo, *Proceedings of the National Academy of Sciences* **112**, 7045 (2015).
- [33] K. C. Leptos, M. Chioccioli, S. Furlan, A. I. Pesci, and R. E. Goldstein, *bioRxiv* (2018), 10.1101/254714, 254714 [10.1101].
- [34] J. Arlt, V. A. Martinez, A. Dawson, T. Pilizota, and W. C. Poon, *Nature Communications* **9**, 1 (2018), 1710.08188.
- [35] X. Jin and I. H. Riedel-Kruse, *Proc. Natl. Acad. Sci. USA* **115**, 3698 (2018).
- [36] Y. Huang, A. Xia, G. Yang, and F. Jin, *ACS Synthetic Biology* **7**, 1195 (2018).
- [37] C. Maggi, F. Saglimbeni, M. Dipalo, F. De Angelis, and R. Di Leonardo, *Nature Communications* **6**, 1 (2015).
- [38] C. Lozano, B. ten Hagen, H. Löwen, and C. Bechinger, *Nature Communications* **7**, 12828 (2016), 1609.09814.
- [39] B. Dai, J. Wang, Z. Xiong, X. Zhan, W. Dai, C.-C. Li, S.-P. Feng, and J. Tang, *Nature Nanotechnology* **11** (2016), 10.1038/nnano.2016.187.
- [40] K. Ozasa, J. Lee, S. Song, M. Hara, and M. Maeda, *Lab on a Chip* **11**, 1933 (2011).
- [41] E. Shoji, H. Nishimori, A. Awazu, S. Izumi, and M. Iima, *Journal of the Physical Society of Japan* **83**, 043001 (2014).
- [42] A. T. Lam, K. G. Samuel-Gama, J. Griffin, M. Loeun, L. C. Gerber, Z. Hossain, N. J. Cira, S. A. Lee, and I. H. Riedel-Kruse, *Lab on a Chip* **17**, 1442 (2017).
- [43] A. C. Tsang, A. T. Lam, and I. H. Riedel-Kruse, *Nature Physics* (2018), 10.1038/s41567-018-0277-7.
- [44] D. B. Weibel, P. Garstecki, D. Ryan, W. R. DiLuzio, M. Mayer, J. E. Seto, and G. M. Whitesides, *Proceedings of the National Academy of Sciences* **102**, 11963 (2005).
- [45] J. Dervaux, M. Capellazzi Resta, and P. Brunet, *Nature Physics* **13**, 306 (2016).
- [46] X. Garcia, S. Rafai, and P. Peyla, *Physical Review Letters* **110**, 138106 (2013).
- [47] M. A. Borowitzka, *Journal of Biotechnology* **70**, 313 (1999).
- [48] H. C. Greenwell, L. M. L. Laurens, R. J. Shields, R. W. Lovitt, and K. J. Flynn, *Journal of The Royal Society Interface* **7**, 703 (2010).
- [49] S. A. Scott, M. P. Davey, J. S. Dennis, I. Horst, C. J. Howe, D. J. Lea-Smith, and A. G. Smith, *Current Opinion in Biotechnology* **21**, 277 (2010).
- [50] E. Harris, *The Chlamydomonas Sourcebook*, *The Chlamydomonas Sourcebook No. v. 2* (Academic, 2009).
- [51] M. Polin, I. Tuval, K. Drescher, J. P. Gollub, and R. E. Goldstein, *Science* **325**, 487 (2009).
- [52] K. W. Foster and R. D. Smyth, *Microbiological reviews* **44**, 572 (1980).
- [53] S. Kateriya, G. Nagel, E. Bamberg, and P. Hegemann, *Physiology* **19**, 133 (2004).
- [54] K. Josef, J. Saranak, and K. W. Foster, *Cell motility and the cytoskeleton* **63**, 758 (2006).
- [55] Z. J. Taylor, R. Gurka, G. A. Kopp, and A. Liberson, *IEEE Transactions on Instrumentation and Measurement* **59**, 3262 (2010).
- [56] S. Childress, M. Levandowsky, and E. A. Spiegel, *Journal of Fluid Mechanics* **69**, 591 (1975).
- [57] T. J. Pedley and J. O. Kessler, *Annual Review of Fluid Mechanics* **24**, 313 (1992).
- [58] M. A. Bees and N. A. Hill, *Physics of Fluids* **10**, 1864 (1998).
- [59] T. J. Pedley and J. O. Kessler, *Journal of fluid mechanics* **212**, 155 (1990).
- [60] D. Anderson, J. Tannehill, and R. Pletcher, *Computational Fluid Mechanics and Heat Transfer*, *Series in computational methods in mechanics and thermal sciences* (Hemisphere Publishing Corporation, 1984).
- [61] J. Ferziger and M. Peric, *Computational Methods for Fluid Dynamics* (Springer Berlin Heidelberg, 2001).
- [62] G. De Vahl Davis and I. P. Jones, *International Journal for Numerical Methods in Fluids* **3**, 227 (1983).
- [63] H. Aref, J. R. Blake, M. Budišić, S. S. Cardoso, J. H. Cartwright, H. J. Clercx, K. El Omari, U. Feudel, R. Golestanian, E. Guillard, G. F. Van Heijst, T. S. Krasnopolskaya, Y. Le Guer, R. S. MacKay, V. V. Meleshko, G. Metcalfe, I. Mezić, A. P. De Moura, O. Piro, M. F. Speetjens, R. Sturman, J. L. Thiffeault, and I. Tuval, *Reviews of Modern Physics* **89**, 1 (2017), 1403.2953.
- [64] A. A. F. Mazarei and O. C. O. Sandall, *AIChE Journal* **26**, 154 (1980).
- [65] A. D. Stroock, S. K. W. Dertinger, A. Ajdari, I. Mezic, H. a. Stone, and G. M. Whitesides, *Science (New York, N.Y.)* **295**, 647 (2002).
- [66] R. V. Vincent and N. A. Hill, *Journal of Fluid Mechanics* **327**, 343 (1996).
- [67] C. R. Williams and M. a. Bees, *Journal of Fluid Mechanics* **678**, 41 (2011).
- [68] C. R. Williams and M. A. Bees, *The Journal of experimental biology* **214**, 2398 (2011).
- [69] M. K. Panda and R. Singh, *Physics of Fluids* **28** (2016), 10.1063/1.4948543.
- [70] M. Pushkin and M. A. Bees, in *Biophysics of Infection, Advances in Experimental Medicine and Biology*, edited by M. C. Leake (Springer, 2016) Chap. 12, pp. 193–205.